Vol 17 No 9, September 2008
1674-1056/2008/17(09)/3163-07

Chinese Physics B

© 2008 Chin. Phys. Soc.
and IOP Publishing Ltd

Rapid Communication

Study of superstructure II in multiferroic $BiMnO_3$*

Ge Bing-Hui(葛炳辉), Li Fang-Hua(李方华)†, Li Xue-Ming(李雪明),
Wang Yu-Mei (王玉梅), Chi Zhen-Hua (迟振华), and Jin Chang-Qing (靳常青)

Beijing National Laboratory for Condensed Matter Physics, Institute of Physics, Chinese Academy of Sciences, Beijing 100190, *China*

(Received 3 July 2008; revised manuscript received 8 July 2008)

The crystal structure of the minor phase, named superstructure II, existing in multiferroic compound $BiMnO_3$ has been studied by electron diffraction and high-resolution transmission electron microscopy. Domains of major and minor phases coexisting in $BiMnO_3$ were observed in high-resolution electron microscope images. The unit cell of minor phase was determined to be triclinic with the size 4×4×4 times as large as the distorted perovskite subcell. The [111] and $[10\bar{1}]$ projected structure maps of the minor phase have been derived from the corresponding images by means of the image processing. A possible rough three-dimensional (3D) structure model was proposed based on the 3D structural information extracted from the two projected structure maps. Since there is no inversion centre in the proposed model, the minor phase may contribute to the ferroelectric property of $BiMnO_3$.

Keywords: multiferroics, $BiMnO_3$, high-resolution transmission electron microscopy, image processing

PACC: 6116D, 6480G, 7780

1. Introduction

Multiferroic materials, a kind of rare materials existing in nature under a severe physical/chemical condition,[1] attract great interest due to their special physical properties and potential applications.[1,2] $BiMnO_3$ is one of widely studied multiferroic materials showing both ferroelectricity and ferromagnetism below the Curie temperature of about 105 K.[3,4] In the early days it was reported that different from rare-earth manganites, the crystal structure of $BiMnO_3$ at the room temperature is of a highly distorted perovskite type with lattice parameters $a_0 \approx c_0 \approx 0.3935$, $b_0 \approx 0.3989$ nm, $\alpha_0 \approx \gamma_0 \approx 91.46°$, and $\beta_0 \approx 90.96°$.[5] Later a monoclinic superstructure (hereafter named superstructure I) was determined by x-ray[6] and neutron diffraction[7,8] with the above-mentioned distorted perovskite structure as its substructure. The space group of superstructure I was determined to be $C2$[6–8] and lattice parameters $a_{\rm I} = 0.954$, $b_{\rm I} = 0.561$, $c_{\rm I} = 0.986$nm, and $\beta_{\rm I} = 110.7°$.[6] Recently, the structure of $BiMnO_3$ was determined by convergent beam electron diffraction as centrosymmetric with the space group $C2/c$,[9] which was supported further by neutron diffraction study.[10] These raised serious concerns about the multiferroic nature of this phase. However, the coexistence of local structures with space group $C2$ and $P2$ (or $P2_1$) in the bulk $BiMnO_3$ were also reported.[11,12]

Apart from the superstructure I, another polymorph (hereafter named as superstructure II) was detected as a minor phase in $BiMnO_3$ by electron diffraction.[6] Montanari *et al* [13] described it as a triclinic structure with the lattice parameters $a_{\rm II} = 1.362$, $b_{\rm II} = c_{\rm II} = 1.366$nm, $\alpha_{\rm II} = 110.0°$, $\beta_{\rm II} = \gamma_{\rm II} = 108.8°$. The ferromagnetic transition of the minor phase is 107 K, different from that of the major phase having the superstructure I. Yang *et al* [14] analysed the composition of the minor phase by means of electron energy-loss spectroscopy and x-ray energy dispersive analysis. They considered that the formation of superstructure II is related with the ordered oxygen deficiency induced by electron-beam irradiation, and proposed a possible cubic structure model based on the oxygen vacancies without taking the displacement of metal atoms into consideration. The lattice param-

*Project supported by the National Natural Science Foundation of China (Grant No 50672124) and Ministry of Science and Technology (MOST) of China (Grant Nos 2005CB724402 and 2007CB925003).

†Corresponding author. E-mail: Lifh@aphy.iphy.ac.cn

eter of this structure model was assigned to be 1.58 nm, almost four times as large as the edge lengths of the distorted perovskite subcell.

The high-resolution transmission electron microscopy (HRTEM) is more appropriate to study the structures of such crystals consisting of different phases and small domains than x-ray and neutron diffraction. The present paper aims at classifying the ambiguity of superstructure II and obtaining the structural information in some more detail by means of electron diffraction and HRTEM in combination with the image processing.

2. Experiment

Polycrystalline $BiMnO_3$ was synthesized from Bi_2O_3 (Alfa Aesar, 99.99%) and Mn_2O_3 (Alfa Aesar, 99.5%) at 1173 K and 6 GPa for 30 minutes.[15] Specimens for TEM observation were prepared by crushing the bulk material soaked in alcohol in an agate mortar, and the fine fragments were dispersed by suspending in alcohol and then transferred onto a carbon microgrid. The electron diffraction camera length was calibrated with the thin golden film evaporated on the microgrid. Electron diffraction patterns (EDPs) and images were taken with a JEM 2010 high-resolution electron microscope fitted with the LaB_6 filament. The point resolution of microscope is 0.194 nm.

3. Electron diffraction and HRTEM analysis

3.1. Lattice parameters

Two phases were found in $BiMnO_3$ by electron diffraction observation. The unit cell parameters of substructure and superstructure I of the major phase are almost the same as those reported in Refs.[5] and [6–8], respectively. The lattice parameters of the substructure of superstructure II determined from EDPs are $a_0 \approx c_0 \approx 0.394$, $b_0 \approx 0.397$ nm, $\alpha_0 \approx \gamma_0 \approx 89.5°$ and $\beta_0 \approx 89.2°$. They are almost the same as those of the substructure of superstructure I. The lattice parameters of superstructure II are $a = c = 4a_0$, $b = 4b_0$, $\alpha = \gamma = \alpha_0$ and $\beta = \beta_0$. Figure 1 shows the EDPs of the minor phase taken with incident beam parallel to the zone axes [010], [001] and [111]. For convenience, here and hereafter the indexes of reflections and zone axes are given according to the substructure. There is no evidence that the symmetry of superstructure II is higher than the triclinic ones.

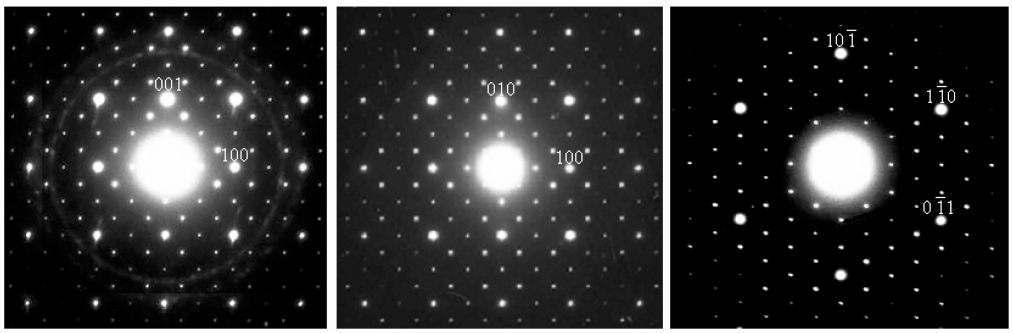

(a) (b) (c)

Fig.1. (a) [010], (b) [001] and (c) [111] EDPs of superstructure II. Reflections are indexed according to the subcell.

3.2. Coexistence of micro domains of two phases

High-resolution electron microscope observation indicates that there are many domains with sizes from several to tens of nanometres in $BiMnO_3$. Figure 2 shows one of the high-resolution electron microscope images of $BiMnO_3$. The diffractograms obtained by Fourier transforming the framed areas A, B and C are inset on the right from the top to bottom, respectively. The analysis of diffractograms indicates that the top and middle ones labelled A and B fit superstructure I and II (see the Roman number on their bottom right), respectively. The fact that the bottom diffractogram labelled C can be obtained by summing up the two others indicates that the micro domains of the major and minor phases are overlapped each other in the top left region in Fig.2.

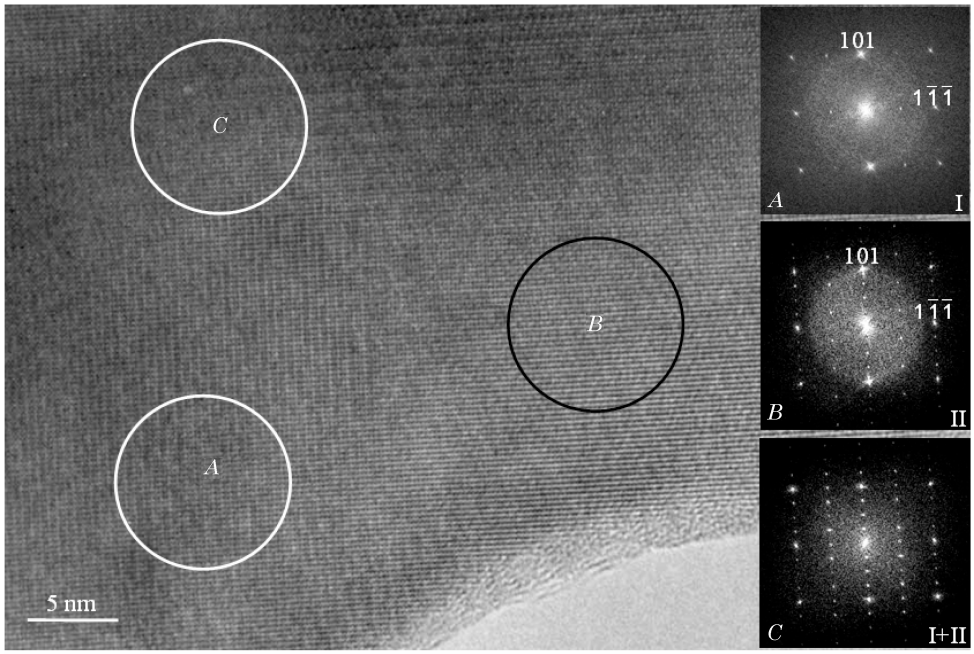

Fig.2. $[12\bar{1}]$ image with the diffractograms corresponding to the framed areas A, B and C inset on the right. The Roman number I or II inset on the bottom right of the diffractogram denotes superstructure I or II, respectively.

3.3. [111] image of the minor phase

Figure 3 shows the [111] image of $BiMnO_3$, which corresponds to the EDP given in Fig.1(c). Fourier transform was carried out for different selected areas, and the diffractograms corresponding to areas A, B and C are inserted on the right from the top to bottom and labelled accordingly. The diffractogram A contains only the strong reflections corresponding to [111] zone of the substructure. The diffractograms B and C are in agreement with the EDP shown in Fig.1(c). Thus the image area A corresponds to the major phase,[13,14] while image areas B and C correspond to the minor phase. The difference of reflection intensities in the diffractogram B from those in C is due to the dynamical electron scattering effect. This effect generally leads to a relative intensity increase of weak reflections and at present is stronger on the thicker area C than the thinner area B. It should be mentioned that the superstructure reflections appeared gradually in the process of observation, namely, the minor phase having the superstructure II is transformed from the major phase having the superstructure I after a long-time electron irradiation. This is in agreement with the report given in Ref.[14].

3.4. $[10\bar{1}]$ image of the minor phase

Figures 4(a) and 4(b) show the image of $BiMnO_3$ taken with the incident beam parallel to the $[10\bar{1}]$ direction of the substructure and the corresponding EDP, respectively. For the convenience of comparison the typical $[10\bar{1}]$ EDP of the minor phase and $[01\bar{1}]$ EDP of the major phase are shown in Figs.4(c) and 4(d), respectively. Again the Fourier transform was performed for different areas, and the diffractograms of areas A and B are inserted on the top and bottom left of the image, respectively. The former is in agreement with the EDP corresponding to a big region of the image given in Fig.4(b), while the latter is identical to the $[10\bar{1}]$ EDP of the minor phase shown in Fig.4(c). By comparing the three EDPs given in Figs.4(b), 4(c) and 4(d), it is seen that the EDP shown in Fig.4(b) is a superposition of the EDPs given in Figs.4(c) and 4(d). Therefore, the image given in Fig.4(a) is composed of $[10\bar{1}]$ domain of the minor phase and $[01\bar{1}]$ domain of the major phase.

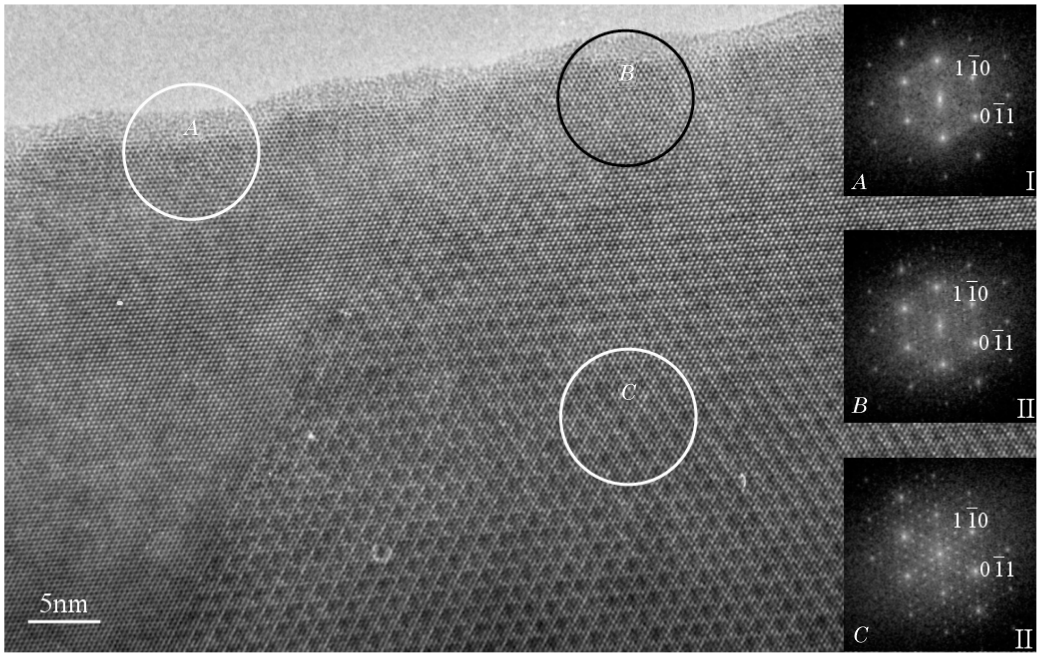

Fig.3. [111] image with the diffractograms corresponding to the framed areas A, B and C inset on the right. The Roman number I or II inset on the bottom right of the diffractogram denotes superstructure I or II, respectively.

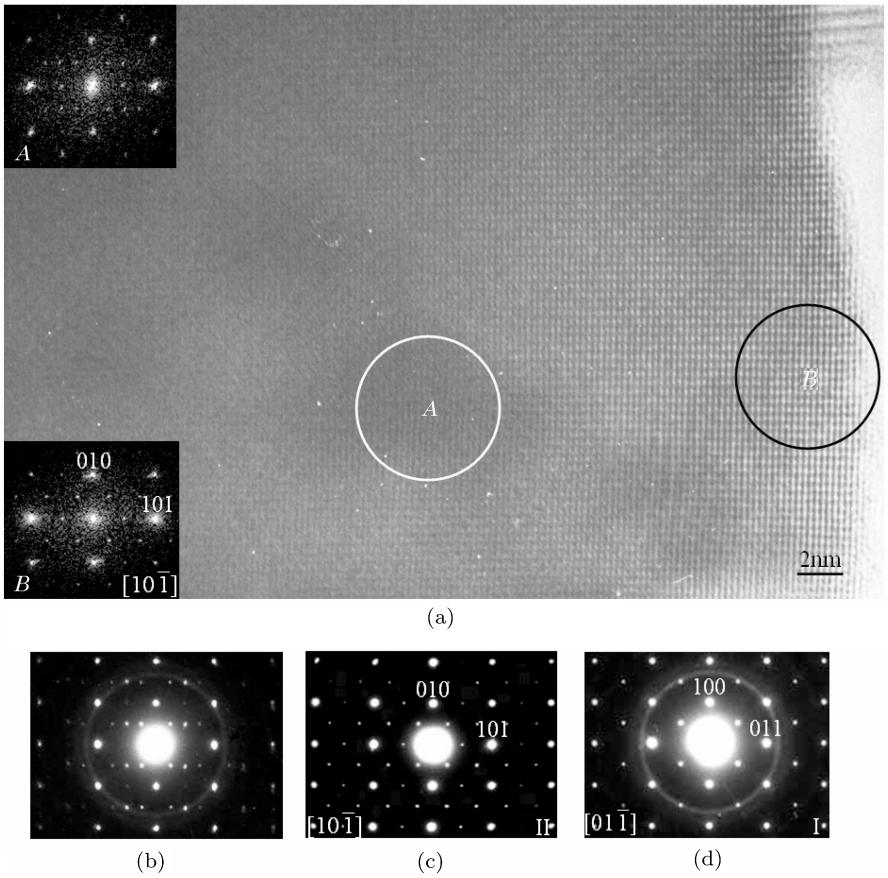

Fig.4. (a) [10$\bar{1}$] image with the diffractograms corresponding to the framed areas A and B inset on the left, (b) the corresponding EDP, (c) [10$\bar{1}$] EDP of superstructure II and (d) [01$\bar{1}$] EDP of superstructure I.

4. Projected structure maps

4.1. Transforming experimental images into projected structure maps

In the process of image formation in HRTEM, the image wave is modulated by the contrast transfer function so that images may not directly reflect the projected structures of examined samples. Fortunately, the image that does not directly or faithfully reflect the crystal structure can be transformed into the structure map by a technique of image processing, named image deconvolution.[16,17] The resolution of such obtained structure map, named also deconvoluted image, is close to the information limit of the microscope. Atoms with the atomic numbers and interatomic distances not very small can be resolved and appear black in the structure map.

4.2. [111] projected structure

Fourier filtering was performed on area B in Fig.3 to reduce the random noise, and the result is shown in Fig.5(a) with the inset parallelogram denoting the size of projected unit cell. The deconvoluted image (see Fig.5(b)) representing the [111] projected structure of the minor phase was derived from Fig.5(a) with the image defocus value –36 nm that is determined based on the principle of Maximum Entropy.[18] Because the original image (Fig.3) was taken near the Scherzer focus that corresponds to the optimum defocus condition, the deconvoluted image (Fig.5(b)) does not much deviate from the filtered experimental image (Fig.5(a)). According to the idealized perovskite model shown in Fig.5(c), it is known that Bi and Mn atoms align in strings parallel to [111] direction. Hence, each black dot in Fig.5(b) represents a Bi(Mn) atomic column. Since the resolution of deconvoluted image is restricted by the information limit of the LaB_6 electron source, the oxygen atoms are invisible due to the insufficient image resolution and small atomic scattering power. The [111] projected model of superstructure II shown in Fig.5(d) was constructed with the positions of Bi(Mn) atomic columns measured from the positions of black dots in Fig.5(b) and the positions of oxygen atoms assigned approximately according to the projected model of idealized perovskite structure as shown in Fig.5(c). The image simulation was carried out based on the model given in Fig.5(d) with different crystal thickness and image defocus values. Other simulation parameters are the acceleration voltage U=200 kV, spherical aberration coefficient C_s=0.5 mm and defocus spread due to the chromatic aberration D=7 nm. The image simulated with defocus value –36 nm and crystal thickness 3.42 nm is shown in Fig.5(e). This image fits the filtered image shown in Fig.5(a) in positions of black dots. In order to interpret the obvious blackness fluctuation of dots in Fig.5(b), the deconvolution was performed on the simulated image given in Fig.5(e), and the corresponding deconvoluted image is shown in Fig.5(f). It is interesting that the agreement of blackness fluctuation of black dots in Fig.5(f) with that in Fig.5(b) is very well. This indicates that the position

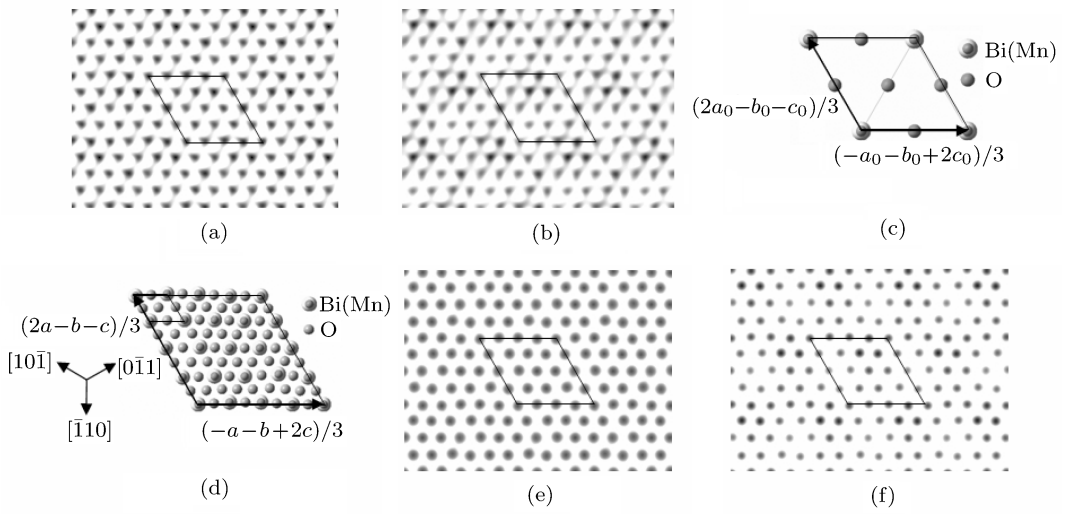

Fig.5. (a) [111] filtered image corresponding to area B in Fig.3, (b) deconvoluted image obtained from (a), (c) and (d) [111] projected structure models of idealized perovskite structure and superstructure II, respectively, (e) image simulated based on the model given in (d), and (f) the deconvoluted image corresponding to (e). The parallelograms in all images denote the projected unit cells and small one in (d) indicates the size of subcell.

deviation of Bi(Mn) atomic columns from the substructure causes not only the displacement of black dots in the image, but also the blackness. Therefore, the [111] projected structure model given in Fig.5(d) seems to be reasonable. However, the deviation of Fig.5(e) from Fig.5(a) and that of Fig.5(f) from Fig.5(b) in the shape of black dots remain to be interpreted. Empirically, it is easy but tedious to match the simulated image with the experimental one by approximately regulating the positions of Bi and Mn atoms in the structure model. This will be discussed in section 4.4.

4.3. $[10\bar{1}]$ projected structure

Figure 6(a) shows the Fourier filtered image of area B shown in Fig.4(a) with the rectangle indicating the projected unit cell. The image defocus was determined to be –37 nm and the derived deconvoluted image is shown in Fig.6(b). Big and small black dots seen in the deconvoluted image denote Bi(O) and Mn atomic columns, respectively. The model of $[10\bar{1}]$ projected structure shown in Fig.6(c) was reconstructed with the positions of Bi(O) and Mn atomic columns measured from Fig.6(b) and those of oxygen atoms are assigned approximately according to the idealized perovskite structure, of which the model is given in Fig.6(d). Here the argument concerning the deviation of black dots from the substructure in both the positions and contrast for the [111] image is also available. The image simulated based on the model given in Fig.6(c) with the crystal thickness 3.36 nm and defocus value –37 nm matches the filtered experimental image given in Fig.6(a) very well. Because atoms of Bi(O) and Mn are not overlapped in the $[10\bar{1}]$direction, the position deviation of the two kinds of atoms from the substructure can be separately seen.

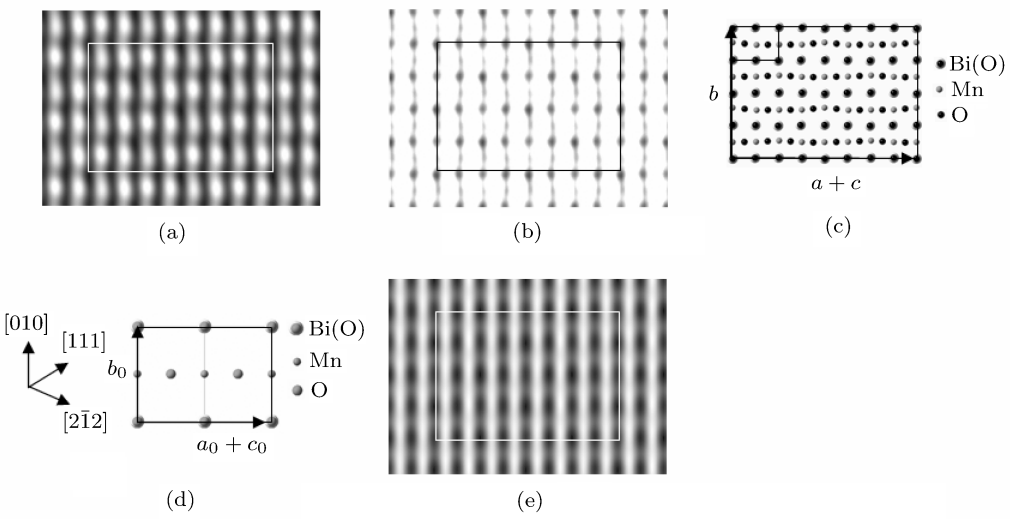

Fig.6. (a) $[10\bar{1}]$ filtered image corresponding to area B in Fig.4(a), (b) deconvoluted image obtained from (a), (c) and (d) $[10\bar{1}]$ projected structure models of superstructure II and idealized perovskite structure, respectively, (e) image simulated based on the model given in (c). The rectangles in all images denote the projected unit cells and small one in (c) indicates the size of subcell.

4.4. Three-dimensional structural information

Though the two determined projected structure maps are insufficient for deriving a perfect three-dimensional (3D) structure, some important 3D structural information can be extracted from the two maps. Figure 5(b) gives evidence that the superstructure II is a huge distorted perovskite structure with the unit cell composed of 4×4×4 distorted perovskite subcells. As mentioned above the simulated image given in Fig.5(e) fits Fig.5(a) only in positions of black dots but not in shapes. The fact that all black dots in Figs.5(a) and 5(b) are shaped in triangle with the three apexes pointed to $[\bar{1}10]$, $[0\bar{1}1]$ and $[10\bar{1}]$ directions (see the bottom left in Fig.5(d)), respectively, implies a small shift of Bi and Mn atoms in three directions related to the three above mentioned ones. Suppose the three directions are parallel to zone axes $[\bar{1}31]$, $[1\bar{1}3]$ and $[31\bar{1}]$, of which the projections onto the (111) plane are parallel to $[\bar{1}10]$, $[0\bar{1}1]$ and $[10\bar{1}]$ directions, respectively. Inside the unit cell of superstructure II each atomic string parallel to the $<111>$ direction consists of four pairs of Bi and Mn atoms. Hence, it can be supposed

that three pairs of atoms shift a small amount in the above mentioned three directions, respectively, while the fourth has a shift along the string or keeps motionless. Such atomic displacement might be caused by the oxygen deficiency as suggested by Ref.[14].

Furthermore, the projections of $[\bar{1}31]$, $[1\bar{1}3]$, and $[31\bar{1}]$ directions onto the $(10\bar{1})$ plane are parallel to [010], $[2\bar{1}2]$ and [111] directions (see the bottom left in Fig.6(d)), respectively. In Fig.6(b) big and small dots representing Bi(O) and Mn atomic columns, respectively, are obviously elongated along the vertical. This can be interpreted by the atomic shifts parallel to the [010] direction. In addition, it seems that black dots can be divided into two groups with one group turning slightly clockwise, while the other anticlockwise. This is in accordance with the atomic shifts parallel to the $[2\bar{1}2]$ and [111] directions, respectively.

The discussion on the 3D structural information extracted from the [111] projected structure map based on the triangular black dots representing Bi(Mn) atomic columns is compatible with the appearance of black dots in the $[10\bar{1}]$ projected structure map. According to the above argument it is reasonable to propose a possible rough 3D structure model as follows. The unit cell of superstructure II is composed of 64 modified distorted perovskite subcells. The modification is mainly in the slight shifts of Bi and Mn atoms. On the whole the atomic shifting makes the arrangement of Bi and Mn atoms approximately follow a local three-fold symmetry. This interprets the appearance of atomic columns in the [111] projected structure map as triangular black dots. Evidently, there is no inversion centre in such structure model of superstructure II and hence the minor phase may contribute to the ferroelectric property of $BiMnO_3$. The results may be helpful to understand the controversy over the origin of multiferroics of $BiMnO_3$ compounds.

5. Conclusions

Electron diffraction and HRTEM study indicates that there are two phases coexisting in $BiMnO_3$. The domains of major and minor phases were identified by means of the diffractograms obtained by selected-area Fourier transform. It was determined that the superstructure II in $BiMnO_3$ has a huge triclinic unit cell composed of $4\times4\times4$ distorted perovskite subcells. The image deconvolution technique was utilized to obtain the [111] and $[10\bar{1}]$ projected structure maps with Bi and Mn atomic columns appearing as big and small black dots, respectively. Based on the 3D structural information extracted from the two projected structure maps, a possible rough 3D structure model was proposed. In this model the distorted perovskite subcells are modified by shifting three Bi and Mn atoms along the $[\bar{1}31]$, $[1\bar{1}3]$, and $[31\bar{1}]$ directions, such that the projections of Bi and Mn atoms in the [111] direction approximately follow a local three-fold symmetry. This model is non-centre symmetrical, hence we suggest the minor phase may contribute to the ferroelectric property of $BiMnO_3$.

References

[1] Hill N A 2000 *J. Phys. Chem.* B **104** 6694
[2] Schmid H 1994 *Ferroelectrics* **162** 317
[3] dos Santos A M, Parashar S, Raju A R, Zhao Y S, Cheetham A K and Rao C N R 2002 *Solid State Commun.* **122** 49
[4] Kimura T, Kawamoto S, Yamada I, Azuma M, Takano M and Tokura Y 2003 *Phys. Rev.* B **67** 180401(R)
[5] Sugawara F, Iiida S, Syono Y and Akimoto S 1968 *J. Phys. Soc. Jpn.* **25** 1553
[6] Chiba H, Atou T, Faqir H, Kikuchi M, Syono Y, Murakami Y and Shindo D 1998 *Solid State Ionics* **108** 193
[7] Atou T, Chiba H, Ohoyama K, Yamaguchi Y and Syono Y 1999 *J. Solid State Chem.* **145** 639
[8] dos Santos A M, Cheetham A K, Atou T, Syono Y, Yamaguchi Y, Ohoyama K, Chiba H and Rao C N R 2002 *Phys. Rev.* B **66** 064425
[9] Belik A A, Iikubo S, Yokosawa T, Kodama K, Igawa N, Shamoto S, Azuma M, Takano M, Kimoto K, Matsui Y and Takayama-Muromachi E 2007 *J. Am. Chem. Soc.* **129** 971
[10] Montanari E, Calestani G, Righi L, Gilioli E, Bolzoni F, Knight K S and Radaelli P G 2007 *Phys. Rev.* B **75** 220101
[11] Kodama K, Iikubo S, Shamoto S I, Belik A A and Takayama-Muromachi E 2007 *J. Phys. Soc. Jpn.* **76** 124605
[12] Yokosawa T, Belik A A, Asaka T, Kimoto K, Takayama-Muromachi E and Matsui Y 2008 *Phys. Rev.* B **77** 024111
[13] Montanari E, Righi L, Calestani G, Migliori A, Gilioli E and Bolzoni F 2005 *Chem. Mater.* **17** 1765
[14] Yang H, Chi Z H, Li F Y, Jin C Q and Yu R C 2006 *Phys. Rev.* B **73** 024114
[15] Chi Z H, Xiao C J, Feng S M, Li F Y, Jin C Q, Wang X J, Chen R Z and Li L T 2005 *J. Appl. Phys.* **98** 1031519
[16] Li F H 2003 *Z. Krist.* **218** 279
[17] Tang C Y, Li F H, Wang R, Zou J, Zheng X H and Liang J W 2007 *Phys. Rev.* B **75** 184103
[18] Hu J J and Li F H 1991 *Ultramicroscopy* **35** 339